Isotopic Effects in the Laser Control of Dissociative Ionization at High Intensities: Role of Permanent Dipole Moments†

J. Levesque,‡ S. Chelkowski, and A. D. Bandrauk*,§

Laboratoire de Chimie Théorique, Faculté des Sciences, Université de Sherbrooke, Sherbrooke, Québec J1K 2R1, Canada

Received: September 11, 2002; In Final Form: January 28, 2003

Exact (non-Born−Oppenheimer) numerical solutions of the time-dependent Schrödinger equation for a 1-D model of the one-electron isotopomer systems H_2^+, HD^+, and HT^+ have been obtained in a two-color laser control scheme, $\omega + 2\omega$, of dissociation and dissociative ionization in the high-intensity ($I \geq 10^{13}$ W/cm^2), nonlinear, nonperturbative regime of laser−molecule interaction. Calculations have been performed at the fundamental wavelengths $\lambda_{CO2} = 10.3$ μm and $\lambda_{YAG} = 1.064$ μm in combination with their second harmonics in order to study the effect of laser frequency and permanent dipole moments on the electron−nuclear dynamics in the presence of periodic asymmetric fields. It is found that asymmetries occur in both the ionization and the dissociation. The phase sensitivity is shown to be quite different in the two wavelength regimes. Adiabatic and nonadiabatic quasistatic models of the dissociation and ionization processes are shown to offer simple interpretation of the calculated asymmetries in terms of *tunneling ionization* and *barrier suppression* dissociation.

1. Introduction

Current laser technology is giving experimentalists the access to laser pulses which can be shaped, frequency swept (chirped), and phase controlled, even down to a few cycles and ever increasing intensities.[1] These new pulse intensities are now approaching the intensity corresponding to the atomic unit of electric field ($E_0 = e/a_0^2 = 5 \times 10^9$ V/cm), $I_0 = 3.5 \times 10^{16}$ W/cm^2 (where in atomic units, $\hbar = m_e = e = a_0 = 1$).

The shortness of current pulses, with the recent breaking of the attosecond barrier,[2] gives access in principle to direct measurement of electronic motion in atoms and molecules, whereas increasing intensity allows for manipulation of molecules on the femtosecond time scale.[3] The ultimate goal is the imprinting of *quantum information* into molecular wave functions via appropriately shaped pulses in order to control and guide the spatiotemporal evolution of matter, leading to the optimal control theory of optical processes.[4]

The simplest approach to induce control in time-dependent laser interactions is a superposition of fields of multiple frequencies whose relative phase can be varied continuously. This has led to a perturbative approach of predicting control of molecular dynamics called *coherent control*.[5,6] This form of quantum control is achieved via the phase-dependent interferences of various molecular transition amplitudes induced by external laser fields. Whereas previous approaches have relied on symmetry preservation in multiphoton processes, such as the well-known $\omega + 3\omega$ scheme,[7] nonsymmetry conserving multiphoton processes such as $\omega + 2\omega$ were already proposed to control both spatial and fragment distributions in dissociation.[8,9] Nonsymmetry conserving or "symmetry-breaking" multiphoton processes inherently lead to simultaneous asymmetries in spatial (angular) and product distributions. It has been shown by Haljan et al. that such $\omega + 2\omega$ superpositions could be used to obtain an extensive control over dissociation dynamics of homonuclear molecular ions, by controlling the electron localization in the molecule.[10] The phase dependence of these distributions can be further quantified in the perturbative regime by examining the actual photon number dependence of the total multiphoton process by Fourier transforming the phase- dependent (ϕ-dependent) transition amplitude $T(\phi)$ with respect to ϕ, giving the nth photon contribution T_n to be the total control process[9] since the photon number n and the phase ϕ are conjugate variables which do not commute in the quantum regime.[11]

Intense fields approaching the atomic unit of electric field (E_0) induce radiative transitions which will be faster than picosecond radiationless relaxation times in molecules. Thus a transition moment μ of one atomic unit interacting with an electric field E_0 of one atomic unit gives the atomic unit of Rabi frequency, $\omega_R = E\mu = eE_0a_0 = 27.2$ eV. This in turn corresponds to the atomic unit of transition time, $\tau_0 = 24.2 \times 10^{-18}$ s $\simeq$ 24 as. At the intensities that we shall consider, $I \approx 10^{14}$ W/cm^2, transition times τ of less than 1 fs will be induced per atomic unit of transition moment. Clearly such rapid radiative transitions will initially produce large molecular coherences. Unfortunately, although intensities of 10^{14} W/cm^2 are 2 orders of magnitudes lower than I_0, the corresponding electric field E is but 1 order of magnitude lower than the atomic unit $E_0 = 5 \times 10^9$ V/cm, which is a measure of electric fields inside atoms and molecules (i.e. $E/E_0 \approx 10^{-1}$). Such field strengths, which are now commonly attained by experimentalists, are in the nonperturbative regime and will induce ionization. In the low-frequency, long-wavelength regime (e.g. $\lambda_{CO2} = 10.6$ μm), ionization rates can be faster than the laser frequency itself (e.g. $\tau_{CO2} = 35$ fs) and can be considered to occur at the peak

† Part of the special issue "George S. Hammond & Michael Kasha Festschrift." In honor of M. Kasha.

* To whom correspondence should be adressed. E-mail: andre.bandrauk@courrier.usherb.ca.

‡ Present address: INRS Énergie-Matériaux, Varennes, Québec J3X 1S2, Canada.

§ Canada Research Chair in Computational Chemistry and Photonics.

10.1021/jp022044v CCC: $25.00
Published on Web 04/01/2003

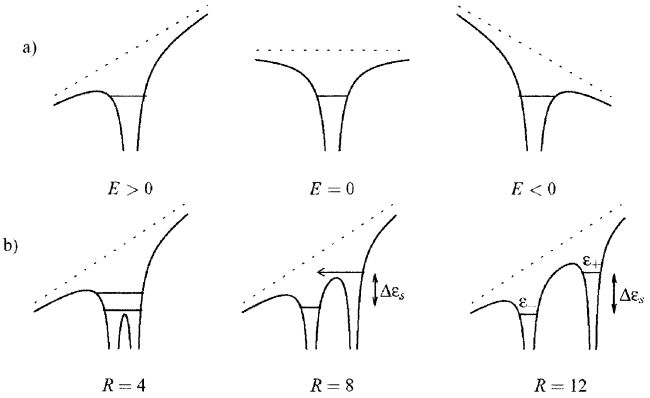

Figure 1. (a) Atomic electronic potentials distorted respectively by the presence of a strong positive, null, and negative external electric field. (b) Electronic molecular ptoentials in a positive electric field, as a function of the internuclear distance R. The Stark shift $\Delta\epsilon_S$ between the two localized molecular orbitals ϵ_+ and $\epsilon_- \simeq E_{max}R$.

of the field. This leads to a quasistatic tunneling model to calculate ionization rates[12,13] and other processes such as high-order harmonic generation, HOHG.[14] Such a quasistatic model leads to the definition of a parameter, called the Keldysh parameter,[12,13] γ, which separates quasistatic tunneling ionization processes from high-order perturbative multiphoton transitions:

$$\gamma = \sqrt{\frac{I_p}{2U_p}}, \quad U_p = \frac{E_{max}^2}{4m\omega^2} \tag{1}$$

where I_p is the ionization potential, U_p the ponderomotive (oscillatory) or average energy of a free particle of mass m in a field of maximum amplitude E_{max}, and ω frequency. Physically, γ can be defined also as the ratio of the tunneling frequency ω_t and the laser frequency ω.[15] The tunneling in atoms occurs across the static barrier (Figure 1a) created at the peak field amplitude E_{max} by the combined electron Coulomb potential $-q/r$ in the presence of a nucleus of atomic number q and the electrostatic potential $-E_{max}z$. At very high intensities, complete ionization will occur. By equating the electron bound state energy $-I_p$ to the maximum of the barrier gives the critical electric field intensity E_c required for overbarrier ionization,

$$E_c = I_p^2/4q \tag{2}$$

In the case of the H atom, for which $I_p = 0.5$ au and $q = 1$, this yields $E_c \simeq 3 \times 10^8$ V/cm, corresponding to an intensity of $I = cE_c^2/8\pi = 1.4 \times 10^{14}$ W/cm^2, where c is the velocity of light. Numerical solutions of the time-dependent Schrödinger equation (TDSE) for the H atom in low-frequency fields support this separation of underbarrier static tunneling ionization and overbarrier ionization regimes.[16]

First 3-D numerical simulations of the TDSE for H_2^+ with fixed nuclei showed the existence of enhanced ionization rates at large internuclear distances, exceeding the rates of the H atom by about 1 order of magnitude.[17] These were later confirmed in more detailed 3-D[18,19] and 1-D with fixed[20] and moving (non-Born−Oppenheimer) nuclei calculations[21] of the appropriate TDSE. A quasistatic picture of over-barrier ionization was shown to explain such enhanced ionization,[20,22] called charge resonance enhanced ionization (CREI), which is due to the strong radiative coupling of charge resonance, or charge-transfer processes in molecules as suggested first by Mulliken.[23] Thus, as shown in Figure 1b for molecules, the HOMO ($1\sigma_g$) and LUMO ($1\sigma_u$) become Stark shifted orbitals $1\sigma_-$ and $1\sigma_+$, with energies ϵ_- and ϵ_+, at the peak of the field E_{max}. At large R, the energy separation between these is $E_{max}R$, i.e. the potential energy difference between atom a, where $1\sigma_-$ becomes the atomic orbital $1s_a$, and atom b, where $1\sigma_+ = 1s_b$.

Evaluating the critical distance R_c where the LUMO energy ϵ_+ coincides with the top of the internal total barrier, $V_c + E_{max}z$, where V_c is the electron−nuclear Coulomb potential, allows for the prediction that $R_c = 4/I_p$ in H_2^{+}[20] and $R_c = 5/I_p$ in linear H_3^{2+},[24] in agreement with 3-D numerical calculations. At distances $R > R_c$, one sees from Figure 1b that the LUMO ($1\sigma_+$) is trapped by the middle barrier, thus inhibiting ionization and creating a sharp drop of the ionization rate, down to the asymptotic value corresponding to the H atom. The phenomenon of enhanced ionization has been found also in nonlinear molecules such as H_3^{2+}; i.e. a critical bond length R_c and critical angle θ_c exist where the laser excited LUMO is above all internal electrostatic barriers of the molecule at the peak field E_{max}.[25] Recently exact nonperturbative calculations of the two-electron systems H_2 and linear H_3^{+}[26] have shown that enhanced ionization occurs also at critical distances due to complete transfer of one-electron from one end of the molecule to the other and is highly controlled by electron correlation. This type of transition was predicted by Mulliken and called *charge resonance transitions*.[23] Similar charge-transfer models as for H_2^{+}[20,24] lead to simple expressions for R_c in the two-electron case.[26] The above-cited references show that quasistatic models of interaction of molecules with intense laser fields lead to the prediction of CREI as a universal phenomenon and offer furthermore a simple explanation for the occurrence of low-energy Coulomb explosion of molecular fragments.[27−29] This phenomenon is due to the fact that Coulomb explosion does not occur by ionization at the equilibrium distance, R_e, but rather at the CREI critical distance R_c discussed above.

In the present work we examine the dissociative ionization by short intense laser pulses in the coherent superposition:

$$E(t) = E_0(t)[\cos(\omega t) + f\cos(2\omega t + \phi)] \tag{3}$$

where $E_0(t)$ is the field envelope, f the relative amplitude, and ϕ the relative phase of the second harmonic field ($\cos(2\omega t)$) with respect to the fundamental frequency. We illustrate in Figure 2a the ratio of the resulting maximum E_{max} and minimum E_{min} as a function of ϕ and f. It is readily seen in this figure that $\phi = 0$ and $f = 0.5$ result in an extremum in the field superposition. Figure 2b shows two cases at $f = 0.5$, $\phi = 0$ and $\phi = \pi/2$. This shows that the coherent superposition in eq 3 produces fields that are periodic, but locally nonsymmetric. In the perturbative multiphoton regime this results in total symmetry-breaking transitions with resulting asymmetries in angular distributions.[8,9] Intense field atomic ionization with field superpositions as in eq 3 revealed early on anomalies in the angular distributions.[30] These were confirmed further in the molecular case, initially by Sheehy et al.[31] and then by Thompson et al.[32] It was found that, in the molecular cases of H_2 and HD, electrons and protons during the dissociative ionization process are preferentially emitted in the same direction, a rather "counterintuitive" or "nonclassical" result. Exact numerical solutions (non-Born−Oppenheimer) of the TDSE for the 1-D H_2^+ system performed by our group confirmed this counterintuitive result,[33,34] but contrary to the original physical interpretation,[31,32] this nonclassical behavior of the electron−proton system at high intensity was shown to be the result of "*tunneling*" ionization of the electron rather than anomalous dissociation of the proton.

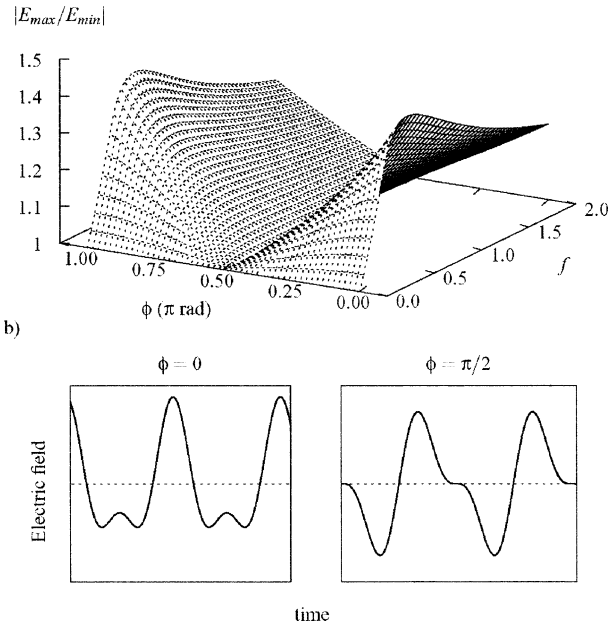

Figure 2. Total field $E(t)$ (eq 3): (a) Ratio of maximum, E_{max} and minimum E_{min} field amplitudes as a function of phase ϕ and relative amplitude f; (b) ratio $E(t)/E_0$ for phases $\phi = 0$ and $\phi = \pi/2$, $I_0 = 4.4 \times 10^{13}$ W/cm^2, $f = 0.5$.

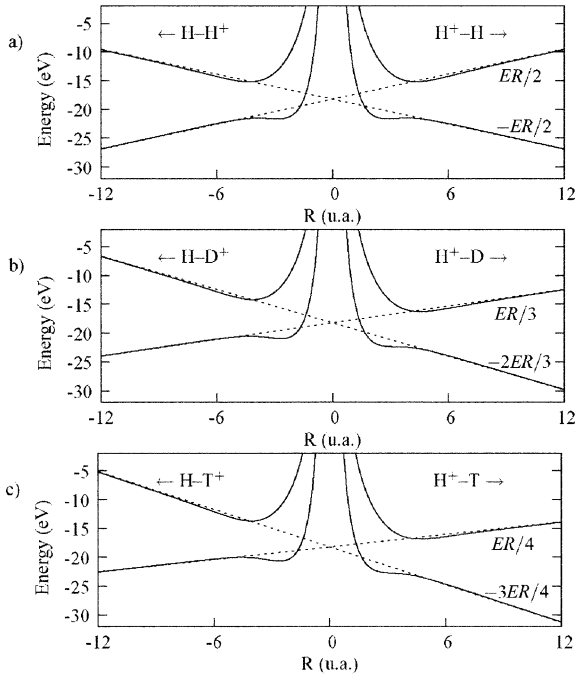

Figure 3. Molecular potentials for (a) H_2^+, (b) HD^+, and (c) HT^+ in a static electric field corresponding to the peak strength E_{max} of a 10^{14} W/cm^2 laser radiation. The figures show both orientations for the field-aligned molecules, so that the positive coordinates correspond to the proton being upfield (H_2^+, DH^+, TH^+), while the negative coordinates show the potentials for the orientation with the proton downfield (H_2^+, HD^+, HT^+).

As we will show below by exact non-Born−Oppenheimer simulations of the TDSE in 1-D for the isotopomers H_2^+, HD^+, and HT^+, anomalies of dissociative ionization of simple molecules in intense short laser pulses can be explained in terms of *quasistatic* models for both ionization[33,34] and dissociation.[35,36] We have discussed above quasistatic models of CREI for ionization of electrons based on Stark displacements of the LUMO through nonperturbative field coupling with the HOMO. In the case of dissociation only, such field couplings of the HOMO and LUMO lead to *barrier suppression* models of dissociation in strong static fields.[35−38] Thus as illustrated in Figure 3 for the three isotopomers H_2^+, HD^+, and HT^+, the presence of permanent dipole moments in the latter two automatically induces asymmetries in the dissociation when the purely electron-field interaction in H_2^+ (Figure 3a) is coupled with the permanent dipoles (Figure 3b,c). Comparison of exact simulations of dissociative ionization of H_2^+, HD^+, and HT^+ will help us establish the competition between permanent dipole, electronic, and non-Born−Oppenheimer effects in this new regime of modern photochemistry—the nonlinear, nonperturbative laser−molecule interaction regime.

2. 1-D Models and Numerical Methods

H_2^+. We have previously solved numerically the complete three-body, 3-D TDSE with both electronic and nuclear degrees of freedom included,[19] i.e., an exact non-Born−Oppenheimer simulation using absorbing boundaries thus losing information on the high-energy ionized electrons and the accompanying dissociated nuclei. We now solve the exact 1-D problem avoiding absorbing boundaries as follows:[21]

$$i\frac{\partial\psi(z,R,t)}{\partial t} = [H_R(R) + V_C(z,R) + H_z(z,t)]\psi(z,R,t) \quad (4)$$

where

$$H_z(z,t) = -\beta\frac{\partial^2}{\partial z^2} + \kappa z E(t), \quad \kappa = 1 + \frac{m_e}{2m_p + m_e} \quad (5)$$

$$H_R(R) = -\frac{1}{m_p}\frac{\partial^2}{\partial R^2} + \frac{1}{R}, \quad \beta = \frac{2m_p + m_e}{4m_p m_e} \quad (6)$$

$$V_c(z,R) = \frac{-1}{\sqrt{(z - R/2)^2 + 1}} + \frac{-1}{\sqrt{(z + R/2)^2 + 1}} \quad (7)$$

m_e and m_p ($m_e = 1$ au) are respectively the electron and the proton masses. The Hamiltonian used in (4) is the *exact* three-body Hamiltonian obtained after separation of the center-of-mass motion in 1-D. H_R is the proton kinetic energy operator with the corresponding potential $1/R$, H_z is the corresponding electronic operator with the field interaction $\kappa z E(t)$, and V_c is a regularized 1-D Coulomb potential which removes singularities. The constant 1 is chosen to match the 3-D ionization rates. It corresponds to the average perpendicular coordinate $\rho = (x^2 + y^2)^{1/2}$ in the 3-D case. We note that, for positive $E(t)$, electrons should be accelerated toward $z < 0$, i.e., downfield (see Figure 1), whereas protons are expected to go upfield ($z > 0$). We have used laser pulses of total duration $t_p = 96$ fs (27 cycles), for the wavelengths $\lambda = 1064$ and 532 nm and also $t_p = 354$ fs at 10.6 and 5.3 μm. The two-color laser electric field used in our simulation is given in eq 3, where $E_0(t)$ is the field envelope (we use a 17.7 fs rise and fall, which correspond to five optical periods at 1064 nm) and ϕ is the relative phase, which can be controlled in the experiment. We set $f = 0.5$, since it gives the largest asymmetry in $E(t)$; see Figure 2. The initial vibrational wave function of H_2^+, at $t = 0$, was varied over various vibrational states as discussed below.

We have obtained numerically the time evolution of the total electron−nuclear wave function $\psi(z,R,t)$ using the split-operator method and a special wave splitting technique,[21] which allows recovery of the probability flux lost usually in absorbing boundary methods thus allowing us to compute the complete electron kinetic energy or ATI (above threshold ionization)

spectra for electrons, proton Coulomb explosion, CE, and the dissociation or ATD (above threshold dissociation) spectra in the H + p channel. More specifically, our technique gives us the total 1-D internal wave function $\psi(z,R,t_f)$ at times $t_f > t_p$. Asymptotic wave functions are obtained by projecting the wave function recovered from an internal region (in which an absorber is placed) onto Volkov waves in the *Er* gauge.[21] Normalized ATI electron spectra[33] are obtained by integrating $|\psi(p,R)|^2$, i.e., the momentum distribution, over the proton coordinate R and multiplying by a Jacobian dp/dE. When $\lambda = 1064$ nm, we usually set the final time $t_f = 36$ cycles $> t_p$ in order to let the bounded part of the molecular wave function enough time to relax, but also to allow both slow electrons and protons to reach the asymptotic region until convergence of the result. For wavelengths such as $\lambda = 10.6$ nm and intensities around 10^{14} W/cm^2, the ponderomotive radius for the free electrons is so important that a reliable calculation of the ATI spectra in such cases would necessitate computational grid sizes exceeding today's computer capabilities.

For the present discussion, the asymmetric proton spectra, in the dissociative or ATD p + H channels, were calculated by projecting the total internal wave functions $\psi_i(z,R,t_f)$ on the ground-state hydrogenic electronic wave function $\phi_{1s}(z - R/2)$ and $\phi_{1s}(z + R/2)$, each representing the initial electronic states, with the electron localized at $z = \pm R/2$, respectively. Thus, we obtain two R-dependent proton (deuteron, triton) functions:

$$\psi\text{-}(R) = \int_{-\infty}^{+\infty} dz\, \phi_{1s}(z - R/2)\, \psi_{in}(z,R,t_f), \tag{8}$$

$$\psi_+(R) = \int_{-\infty}^{+\infty} dz\, \phi_{1s}(z + R/2)\, \psi_{in}(z,R,t_f) \tag{9}$$

where $\psi_+(R)$ represents the proton (deuteron, triton) moving up the maximal field (forward, $z > 0$) with the neutral H-atom moving down the field, and vice versa. Next the Fourier transforms $\chi_\pm(p_R)$ (where p_R is the nucleus momentum) of the asymptotic part of $\psi_+(R)$ were calculated.[21] Thus $|\chi_\pm(p_R)|^2\, dp_r/dE$ represents the forward (backward) kinetic energy spectra of nuclear fragments. The intensity of the two-color laser used in our two-color calculations was $I_\omega = cE_0^2/8\pi = 4.4 \times 10^{13}$ W/cm^2 and the 532 nm laser had intensity $I_{2\omega} = 1.1 \times 10^{13}$ W/cm^2, giving the maximum field $E_0(1 + f)$ when $\phi = 0$. In all the cases presented here, we used $f = 0.5$. The resulting total field has the same peak intensity as a single laser of intensity $I_\omega = 10^{14}$ W/cm^2. Two particular relative phases were chosen: $\phi = 0$ and $\phi = \pi/2$. The corresponding combined electric fields are shown in Figure 2b. The exact ATD spectra (with ionization included) are compared with two-surface calculations using only the HOMO and LUMO, i.e. $1\sigma_g$ and $1\sigma_u$, where no ionization occurs.

DH^+ and TH^+. These two isotopomers differ from H_2^+ described above because their center of mass no longer coincides with the center of charge, so that this creates a permanent dipole moment. Under the influence of intense laser fields, i.e., in the nonlinear, nonperturbative regime considered here, one can expect these dipole moments to have corresponding nonperturbative effects on the dissociative ionization process. We shall follow here the original treatment of Hiskes[37] and Hanson[38] who considered the behavior of these molecules in intense electric fields as early as 40 and 30 years ago. The dissociations of these molecules have also been considered more recently at high intensity without ionization in the context of coherent control scenario for possible isotope separation[39] following early experiments by DiMauro et al.[31] In the present paper we consider the complete dissociative ionization of these isotopomers at the intensities considered before in refs 31 and 32.

We restrict ourselves to the 1-D model of H_2^+. The total Hamiltonian (4), electronic and nuclear, for different nuclear masses m_1 and m_2, now becomes[37,38]

$$\hat{H}(z,R,t) = -\frac{1}{2}\left[\frac{m_1 + m_2}{m_1 m_2}\frac{\partial^2}{\partial R^2} + \frac{M}{m_1 + m_2}\frac{\partial^2}{\partial z^2} + \frac{1}{M}\frac{\partial^2}{\partial R_{CM}{}^2}\right] - \left[\frac{1}{z - (m_2/(m_1 + m_2))R} + \frac{1}{z + (m_1/(m_1 + m_2))R}\right] + \frac{1}{R} - E(t)\left[\left(1 + \frac{1}{m_1 + m_2 + 1}\right)z - \left(\frac{m_2 - m_1}{m_1 + m_2}\right)R + R_{CM}\right] + (z,R) \tag{10}$$

where M is the total mass of the molecular system ($M = m_e + m_1 + m_2$).

This reduces to the total H_2^+ Hamiltonian, eq 4, when $m_1 = m_2 = m_p$. We note immediately the presence of the nuclear dipole moment $((m_2 - m_2)/(m_1 + m_2))R$ for nonsymmetric nuclear systems. The above Hamiltonian is defined in the following coordinate system,[37]

$$\begin{pmatrix} z \\ R \\ R_{CM} \end{pmatrix} = \begin{pmatrix} -\frac{m_1}{m_1 + m_2} & -\frac{m_2}{m_1 + m_2} & 1 \\ 1 & -1 & 0 \\ \frac{m_1}{M} & \frac{m_2}{M} & \frac{1}{M} \end{pmatrix} \begin{pmatrix} r_1 \\ r_2 \\ r_e \end{pmatrix} \tag{11}$$

where R_{CM} is the center of mass of the three-body system, R is the internuclear distance, and z is the position of the electron with respect to the center of mass *of the two nuclei*. The three coordinates r_1, r_2, and r_e are the positions of the three particles in Cartesian coordinates, m_1 and m_2 being the respective masses of the corresponding nuclei and $M = m_1 + m_2 + m_e$, the total mass.

We first note that we are considering $E = E(t)$ as being only time-dependent. The use of this approximation, called the dipole approximation,[11] is justified by the fact that $z/\lambda \ll 1$. Since the center of mass, R_{CM}, motion decouples completely from the dynamics *relative* to the center of mass, the total Hamiltonian we consider is

$$\hat{H}(z,R,t) = -\frac{1}{2}\left[\frac{m_1 + m_2}{m_1 m_2}\frac{\partial^2}{\partial R^2} + \frac{M}{m_1 + m_2}\frac{\partial^2}{\partial z^2}\right] - \left[\frac{1}{z - (m_2/(m_1+m_2))R} + \frac{1}{z + (m_1/(m_1+m_2))R}\right] + \frac{1}{R} - E(t)\left[\left(1 + \frac{1}{m_1 + m_2 + 1}\right)z - \left(\frac{m_2 - m_1}{m_1 + m_2}\right)R\right] + (z,R) \tag{12}$$

This is the 1-D Hamiltonian which is solved numerically to describe the complete dissociative ionization of the three isotopomers H_2^+, HD^+, and HT^+ aligned in the laser field and their respective different orientations, DH^+ and TH^+. Since these are 1-D calculations, i.e., without rotations, we need to consider these different orientations for the nonsymmetric molecules. In fact we have shown previously that using ω_{CO2} and its second harmonic (i.e. wavelengths 10.6 and 5.3 μm) will not produce *orientation* because, in general, the pendular state tunneling frequencies between different orientations fall in the microwave (nanosecond) regime,[40] thus requiring a static field[41] or very complex pulses such as those obtained by optimal control

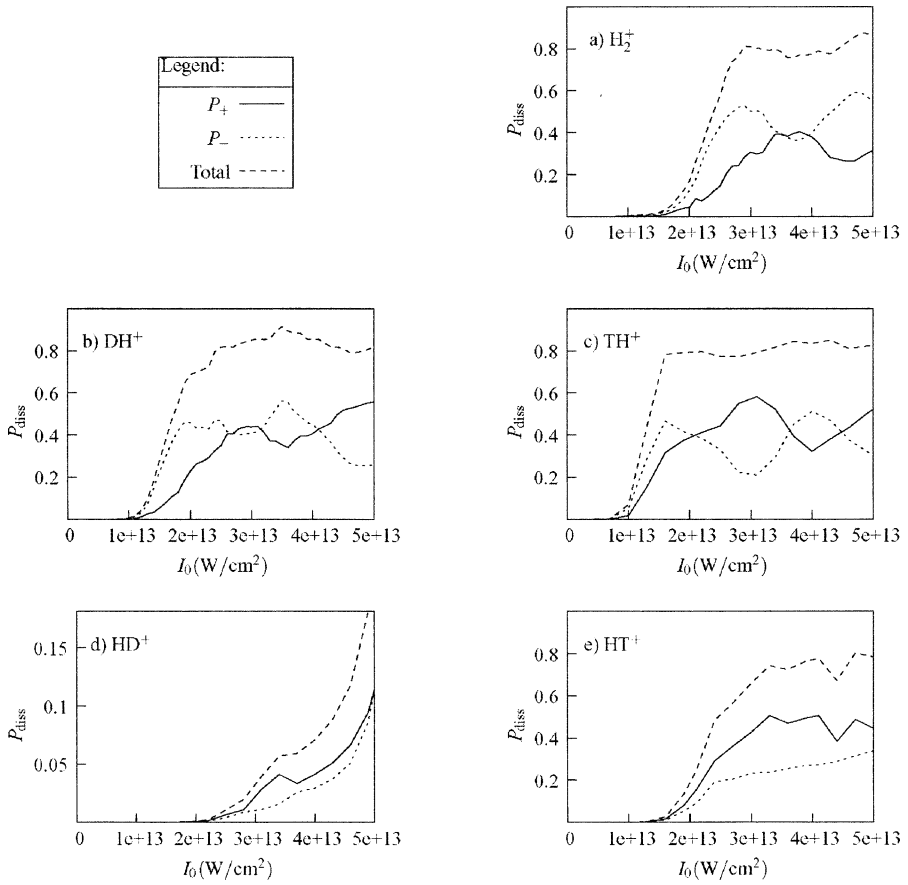

Figure 4. Asymmetry in the dissociation channel obtained for different laser intensities I_0, where $E_0(t)$ is the pulse envelope (eq 3) and with the relative phase $\phi = 0$ between the two laser colors in $\lambda = 10.6 + 5.3$ μm, 350 fs laser pulses. The calculations do not include ionization. Both orientations for each of the field-aligned molecules are shown: (a) H_2^+, (b) DH^+ (proton upfield), (c) TH^+ (proton upfield), (d) HD^+ (deuteron upfield), and (e) HT^+ (triton upfield).

algorithms.[42] The numerical simulations described below will show that prior orientation is not necessary for controlling these systems in a two-color scheme since the different dipole moments under different orientations (see Figure 3) will provide for efficient discrimination between the two orientations.

Thus, upon dissociation, H_2^+ will produce the fragments H + H^+ and H^+ + H with net dipole moments $\pm R/2$. These are purely electronic effects; i.e. they correspond to the transfer of half an electron from one nucleus to the other and are contained in the dipole transition moment $\mu(R) = \langle 1\sigma_g|z|1\sigma_u\rangle = R/2$. HD^+ and DH^+ produce net dipole moments of $R/3$ and $2R/3$, whereas HT^+ and TH^+ will produce net dipole moments of $R/4$ and $3R/4$. Transfer of the electron to the lightest atom H and correspondingly ionization of the heavier atom, D^+ or T^+, lead to always smaller dipole moments. Alternatively, dissociation into H^+ always leads to the largest dipole moment since the proton is farthest from the center of mass. The net effect of this on the dissociation dynamics is that the orientation for which DH^+ and TH^+ are parallel to the maximum positive field ($E > 0$) should undergo much more efficient dissociation due to stronger barrier suppression at low laser frequency[35,36] due to large dipole moments. This is illustrated in Figure 3. Localization of the electron via the radiative interaction coupling of the LUMO ($1\sigma_u$) and HOMO ($1\sigma_g$) orbitals, $\langle 1\sigma_g|zE|1\sigma_u\rangle = \pm E/2R$, leads to the classically expected dipole moment $\pm R/2$ for H + H^+ dissociation. In the case of DH^+, this electronic transition moment R/2, defined with respect to the center of charge, adds to the moment between the center of mass and the center of charge, $R/6$, giving the expected classical dipole moment 2R/3 for $D + H^+$ dissociation, etc.[37,38]

In the next two sections we present calculations of dissociation without ionization (section 3) and with ionization (section 4) for two different wavelengths, $\lambda_{CO2} = 10.6$ μm and $\lambda_{YAG} =$ 1064 nm, superposed with their second harmonic. In the first case the laser period, $t_{CO2} = 35$ fs, is slower than the proton vibration time scale, which in H_2^+ is $t_H = 15$ fs, whereas for the shorter wavelength $t_{YAG} = 3.5$ fs, the laser period is faster than the proton time scale of 15 fs.

3. Asymmetric Dissociation and Ionization in $\omega + 2\omega$ Short Pulses

Using the numerical methods described in the previous section, we report first the asymmetric dissociation probabilities for the long-wavelength, two-color combinations ($\lambda = 10.6 + 5.3$ μm) at relative phases $\phi = 0$ and $\phi = \pi/2$, and relative amplitude $f = 0.5$ as a function of intensity $I_0 = cE_0^2/8\pi$ (see eq 3). Referring to Figure 2b, this corresponds to a maximum intensity $I = I_0(1 + f)^2$. Thus at $I_0 = 4.4 \times 10^{13}$ W/cm^2, the maximum intensity is $I_m = 10^{14}$ W/cm^2. In Figure 4, we report results for H_2^+, DH^+, TH^+, HD^+, and HT^+ for initial vibrational state $\nu_0 = 5$ at $\phi = 0$ and $\phi = \pi/2$ in Figure 5. All calculations were performed for a pulse length of 300 fs. In Figure 6, we illustrate for H_2^+ the evolution of the logarithm of the electronic probability density in the presence of moving nuclei, which has been integrated over all internuclear distances R at times t:

$$|\psi(z,t)|^2 = \int dR|\psi(z,R,t)|^2. \qquad (13)$$

For the latter, with an initial $\nu_0 = 5$ state, the total ionization

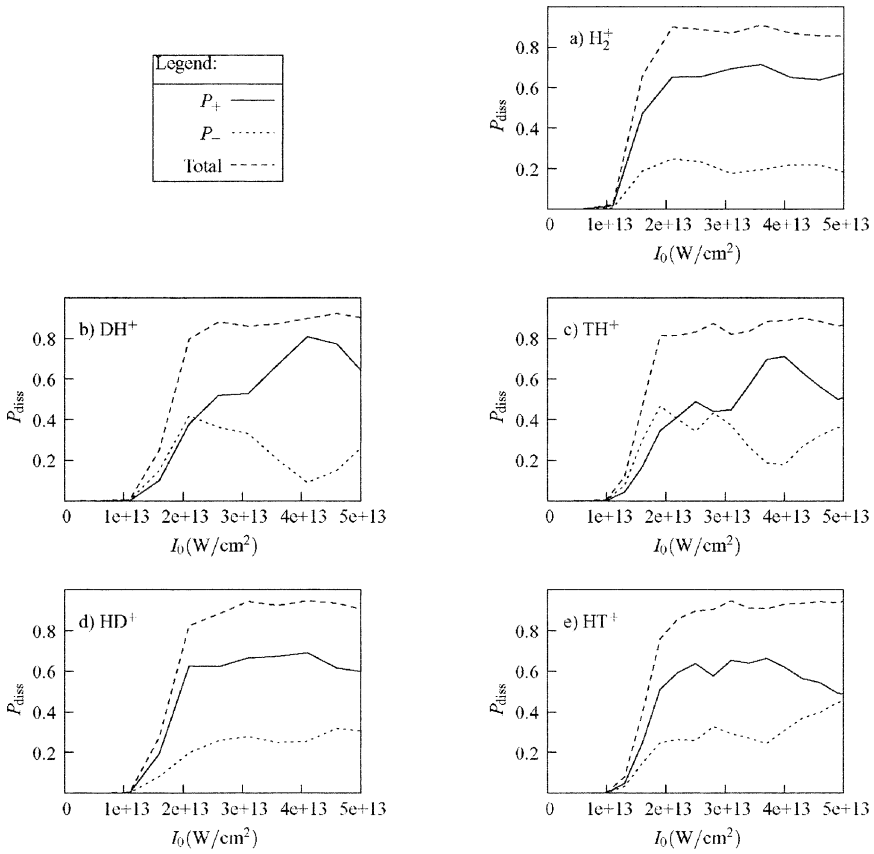

Figure 5. Calculation identical to Figure 4, but with $\phi = \pi/2$.

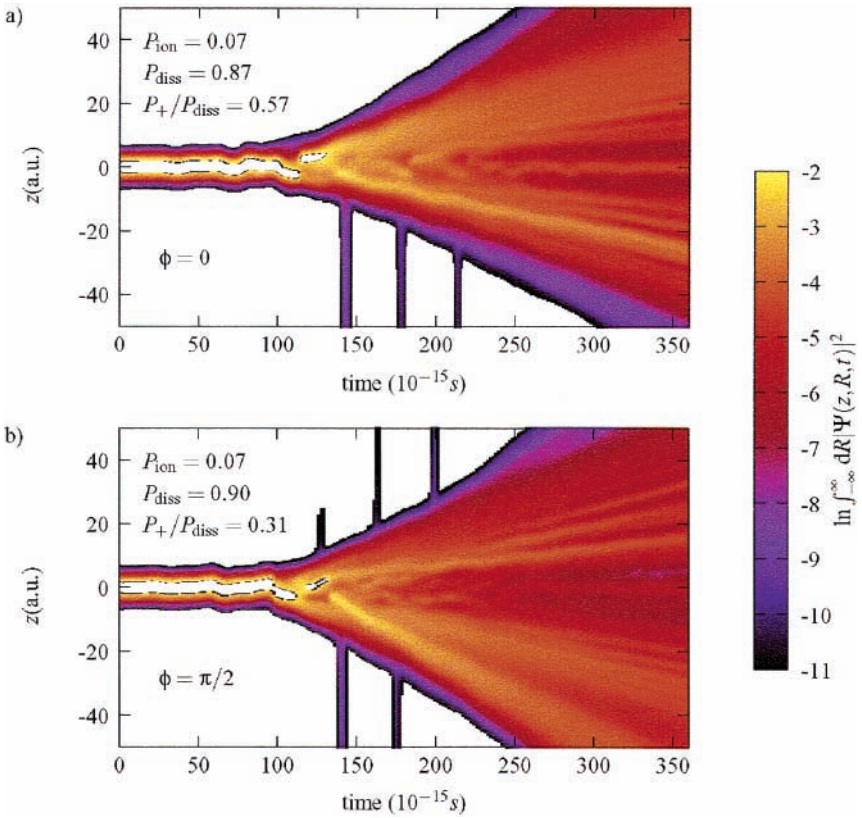

Figure 6. Logarithm of electronic density ($\ln \int_{-\infty}^{+\infty}|\Psi(z,R,t)|^2\, dR$) versus time for H_2^+ in $\lambda = 10.6 + 5.3\ \mu$m, $T = 350$ fs, and $I_0 = 5.0 \times 10^{13}$ W/cm^2 laser pulses: (a) $\phi = 0$; (b) $\phi = \pi/2$. The calculation includes ionization, which is visible from the short ionization bursts happening periodically in the pulses and beginning at the critical distance $R_c \simeq 8$ au.

probability at $I_0 = 5 \times 10^{13}$ W/cm^2 with maximum intensity $I_m = 1.125 \times 10^{14}$ W/cm^2, is $P_{ion} = 0.07$, whereas the total dissociation probability was $P_{diss} = 0.87$ at $\phi = 0$, Figure 6a. The forward to backward dissociation probability in the presence

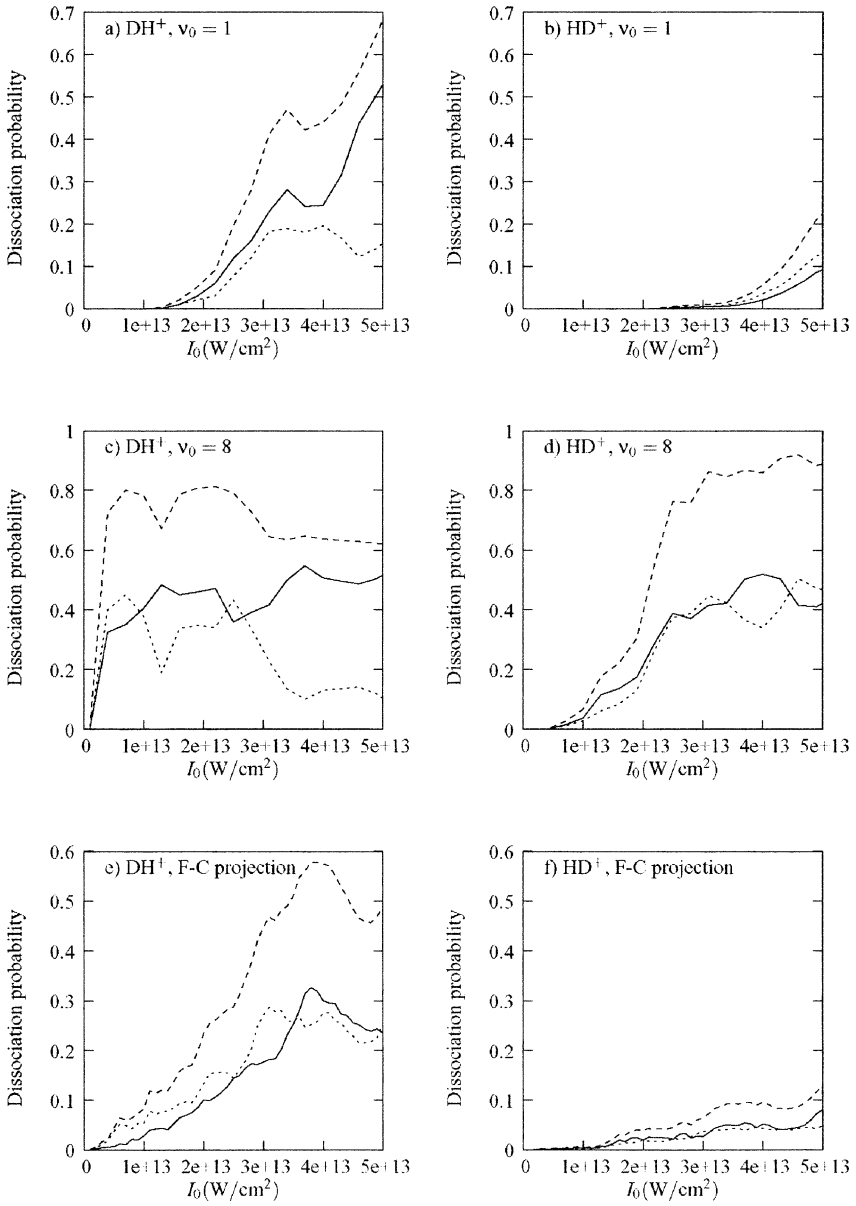

Figure 7. (a) Forward (P_+) and backward (P_-) dissociation probabilities of H_2^+ in a two-color laser pulse (10.6 + 532 μm, $f = 0.5$, 350 fs) for different values of I_0: (a, b) $\nu = 1$; (c, d) $\nu = 8$; (e, f) Franck−Condon projection from the vibrational ground state ($\nu = 0$) of H_2(neutral). Each DH^+/HD^+ couple has been plotted on the same scale.

of 7% ionization for H_2^+ is $P_+/P_- = 0.76$. This compares well with Figure 4, where we report the total dissociation probability of the $\nu_0 = 5$ state of H_2^+ without ionization. A close view of the electron probability illustrated in Figure 6a shows the gradual deflection of electron density on the left proton ($z < 0$) and later then on the right proton ($z > 0$). For $\phi = 0$ bursts of ionization occur at positive maxima of the field for which $E_{max} = 1.5E_0$ (Figure 2a) with electrons ejected backward, i.e., $z < 0$, in accord with classical models, while for $\phi = \pi/2$ (Figure 6b) the ionization occurs equally in both directions, as is expected from the equal maxima/minima at this relative phase (see Figure 2b). Most of the ionization occurs at the critical internuclear distance $R_c \simeq 8$ au ($z = \pm 4$ au) due to CREI, charge resonance enhanced ionization.[18−20]

Inspection of Figure 4, shows the predominance of backward (P_-) products H^+, D^+, and T^+ for H_2^+, DH^+, and TH^+ aligned in the direction of maximum positive field $E_{max} = E_0(1 + f) > 0$ at phase $\phi = 0$. The molecules HD^+ and HT^+, aligned with H downfield ($E < 0$), show the exact opposite behavior, with the dominant product being D^+ and T^+ ejected mainly forward, resulting in the asymmetry $P_+/P_- > 1$. This forward/backward asymmetry in the dissociation of HD^+ and HT^+ diminishes with increasing intensity and is negligible for ν higher than $\nu_0 = 5$. It is to be further noticed that the dissociation probability is always smallest for the HD^+ and HT^+ alignment at lower intensities as compared to H_2^+, DH^+, and TH^+. From the viewpoint of isotope separation using combinations of $\lambda = 10.6$ and 5.3 μm laser pulses, since preferential dissociation occurs with molecules parallel to the laser field due to large electronic and (or) permanent dipole moments in that direction, the dominant dissociation of DH^+/TH^+ into $D^+/T^+ + H$ and that of HD^+/HT^+ into $H + D^+/T^+$ makes this process highly favorable for the lower vibrational states ($\nu < 5$) and intensity $I_0 < 3 \times 10^{13}$ W/cm^2. These optimal conditions as a function of intensity and vibrational state have not been considered before. Figure 7 contains results for other initial vibrational states, $\nu_0 = 1$ and $\nu_0 = 8$, as well as for the initial state corresponding to a Franck−Condon projection from the ground vibrational state of the neutral species H_2. This last case is closely related to experiment, since it corresponds to the

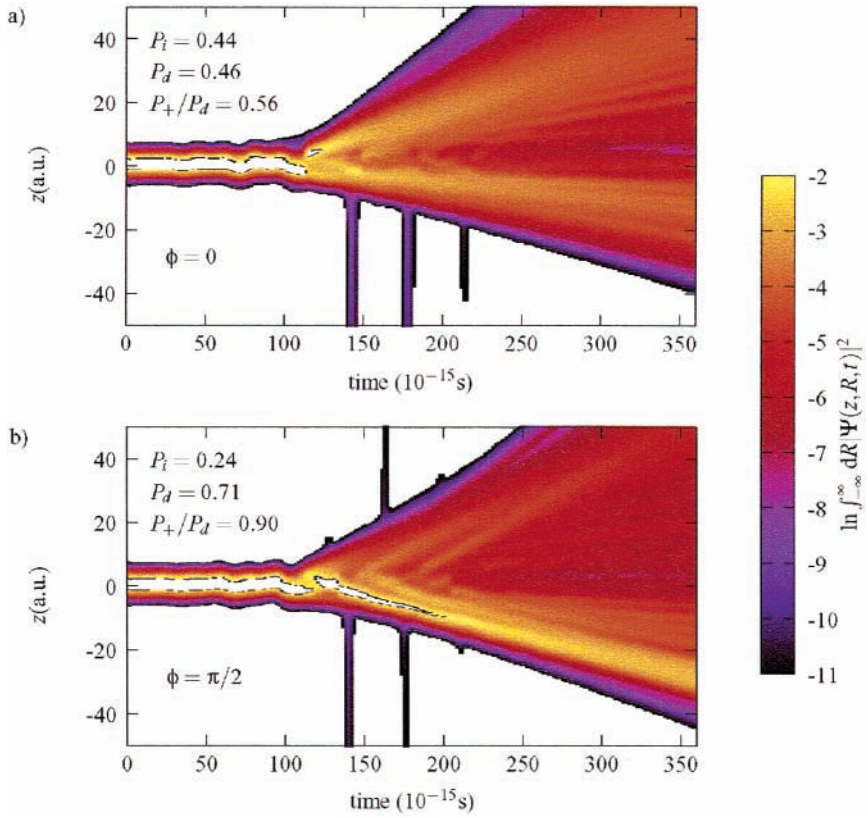

Figure 8. Same parameters as in Figure 6, but for the DH^+ molecular ion (oriented with the proton upfield). Localization of the electron occurs almost equally on both protons in a and mainly on the backward proton ($z < 0$) in b.

mechanism by which H_2^+ is obtained in the laboratory, because of the rapid ionization of H_2 early in the rising of the laser pulse.

Looking at Figure 7e,f, we thus see that to effectively control isotope separation with a CO_2 laser, one has to work in an intensity regime at least below 3.5×10^{13} W/cm^2. At that intensity, the asymmetry ratio for DH^+ indeed starts to change and can even reverse. Such reversals happen for all of the vibrational data shown in Figures 4, 5, and 7. These intensity-dependent variations in the dissociation asymmetry have already been reported for homonuclear molecular ions.[10] For a good control on dissociation, the intensity reached at the focal spot of the laser should thus remain below the intensities where the first reversals appear. Since the asymmetry ratios keep the same forward/backward character below these thresholds, the intensity gradient in the pulse profile should not interfere with isotope separation.

To understand the above results for long-wavelength dissociation using $\omega + 2\omega$ coherent excitation schemes (eq 4), we rely on static models of molecular dissociation at high field strengths.[35−38] The major difference between H_2^+, DH^+, TH^+, HD^+, and HT^+ is the permanent dipole moment in the isotopomers. In a two-surface model, the $1\sigma_g$ and $1\sigma_u$ electronic molecular orbitals and the corresponding molecular potentials $V_g(R)$ and $V_u(R)$ are coupled radiatively by the interaction $\mu(R)E$, where $\mu(R) = R/2$ due to the charge-transfer process.[11] New molecular potentials called *adiabatic* static-field induced potentials are created in the presence of a static field of amplitude E,

$$W_{\pm}(R) = \frac{V_g(R) + V_u(R)}{2} \pm \frac{1}{2}[[V_g(R) - V_u(R)]^2 + (ER)^2]^{1/2} \quad (14)$$

This is illustrated in Figure 3a, where one sees clearly the asymptotes $\pm ER/2$ for H_2^+. In the case of DH^+, TH^+ and HD^+, HT^+, since the center of mass and charge do not coincide, a net nuclear permanent dipole moment can add or subtract to the electronic transition moment $\pm R/2$ as illustrated in Figure 3b,c. Thus, for HD^+ and HT^+ aligned with a positive field ($z > 0$), the asymptotic molecule-field potentials $W_-^{HD^+}(R)$ and $W_-^{HT^+}(R)$ become $-ER/3$ and $-ER/4$, respectively, whereas for opposite alignment, i.e., $W_-^{DH^+}(R)$ and $W_-^{TH^+}(R)$, this becomes $-2ER/3$ and $-3ER/4$. This lowers the dissociation barrier of DH^+ and TH^+ considerably with respect to HD^+ and HT^+ and results in much higher dissociation probabilities for DH^+ and TH^+, as seen in Figures 3b and 4b, by sometimes 2 orders of magnitude at low intensities. The comparable dissociation probabilities of H_2^+, DH^+, and TH^+ as opposed to HD^+ and HT^+ can be related to the similar field-molecule potential $W_-^{H2^+}$ and $W_-^{DH^+}$ (see Figure 3). Thus, the dissociation probabilities follow a quasistatic model termed before as "*barrier suppression*" dissociation.[35,36]

The calculated dominant backward/forward, dissociation probabilities P_-/P_+ for H_2^+, DH^+, and TH^+ reflect electron transfer in the presence of the laser field, with the electron migrating in the opposite direction to the driving field. In the present $\omega + 2\omega$ control scenario, at phase $\phi = 0$ (Figure 2) the maximum field $E_{max} = E_0(1 + f)$ is clearly positive so one would expect a net bias to *forward* H^+ production for H_2^+, DH^+, and TH^+ and much smaller forward D^+, T^+ production for HD^+, HT^+ due to its lower dissociation probability. Figure 4 shows dominant H^+, D^+, and T^+ production for H_2^+, DH^+, and TH^+, whereas D^+ and T^+ is a smaller *forward* dissociation component for $HD^+$and HT^+ at lower intensities. The structure of the $\phi = 0$ field, Figure 2b, shows a more slowly varying and longer negative field component. One can therefore rationalize that the electron will follow *adiabatically* this field component,

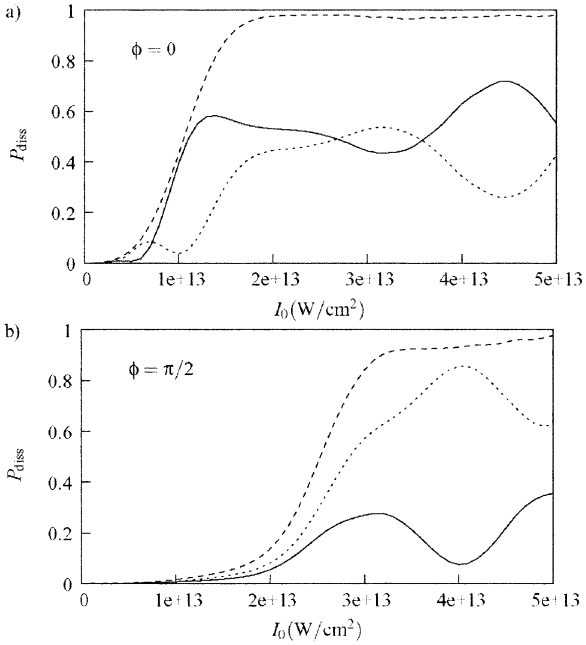

Figure 9. Asymmetry in the dissociation channel for H_2^+, obtained in 100 fs laser pulses with $\lambda = 1064 + 532$ nm and different intensities (i.e. similar to Figures 4 and 5, but using different wavelengths and pulse durations) without ionization: (a) $\phi = 0$; (b) $\phi = \pi/2$.

thus spending more time on the forward nuclei creating preferentially asymmetric molecules H^+H, D^+H, and T^+H. The concertation of the higher dissociation rates and adiabatic electron field transfer in the case of H_2^+, DH^+, and TH^+ can thus explain the dominant backward asymmetry of H^+, D^+, and T^+ production. This interpretation is consistent with the electron density redistribution illustrated in Figure 6a, where somewhat more electronic charges reside in the vicinity of the forward proton ($z > 0$), thus deshielding the backward nucleus ($z < 0$).

Similar reasoning can be applied to the $\phi = \pi/2$ results shown in Figure 5 for $\lambda_{CO2} = 10.6 + 5.3$ μm. At the lower intensities, $I < 2 \times 10^{13}$ W/cm^2, the largest forward/backward asymmetry P_+/P_- is obtained for H_2^+, HD^+, HT^+ (corresponding respectively to the dissociation schemes $H + H^+$, $H + D^+$, and $H + T^+$). This large asymmetry persists at the higher intensities also. Thus at the lower intensities $I < 2 \times 10^{13}$ W/cm^2, one can expect preferential dissociation and isotope separation of the isotopomers HD^+ and HT^+ with D^+ and T^+ ejected mainly in the *forward* direction. This is true also in the case of the mixed initial state shown in Figure 7e,f. By keeping the intensity low enough (below 1×10^{13} W/cm^2 at the focal spot), the difference in the dissociation rates for the two orientations and the dissociation asymmetry in the DH^+ channel would allow significant separation ratios ($P_+/P_{tot.}$). This implies shielding of the backward proton, in agreement with Figure 8b, which shows larger electron population at $z < 0$, on the backward proton, leaving the forward nucleus mostly ionized as the molecule passes through the CREI critical distance $R_c \simeq 8$ au. Figure 4 corresponds to a dissociation calculation where the electronic part of the wave function is approximated as a superposition of the $1\sigma_g$ and $1\sigma_u$ states ("two-surface" calculation) and consequently does not include ionization processes, whereas Figures 6 and 8 correspond to the full dissociative-ionization calculation.

We turn next to the shorter wavelength (or higher frequency) case, $\lambda_{YAG} = 1064 + 532$ nm. In Figure 9a,b, we illustrate the asymmetric dissociation probabilities from a two-surface calculation with no dissociation, for H_2^+ in the $\nu_0 = 5$ initial state and using the relative amplitude $f = 0.5$ with phases $\phi = 0$ and

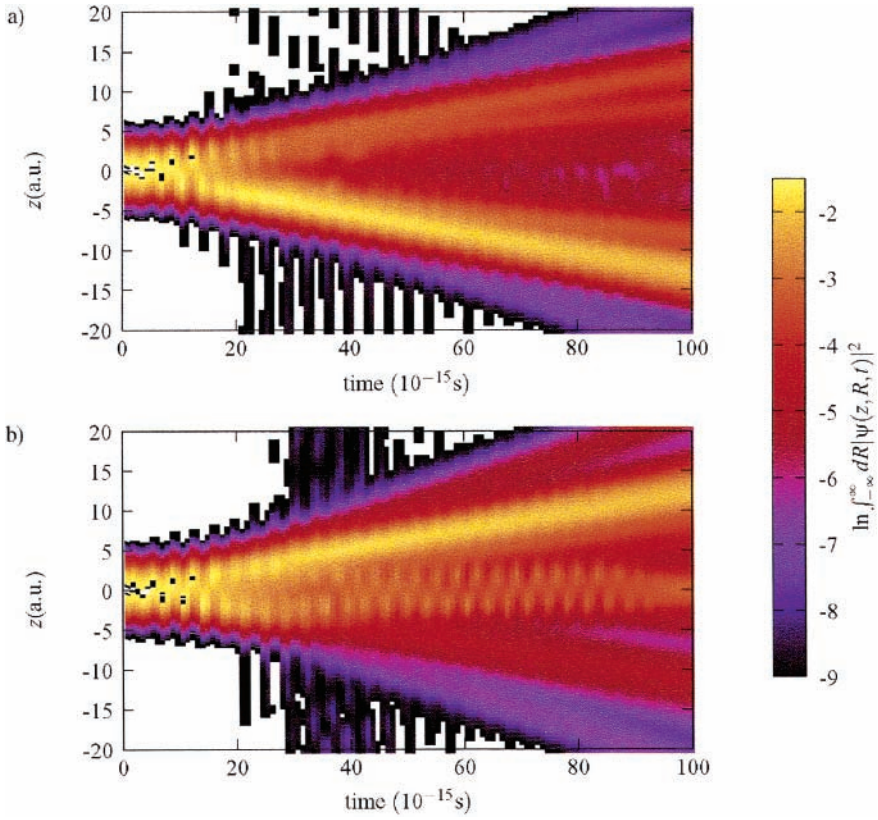

Figure 10. Same as in Figure 6 but with laser parameters $\lambda = 1064 + 532$ nm, $T = 100$ fs, and $I_0 = 4.0 \times 10^{13}$W/cm^2 laser pulses with (a) $\phi = 0$ and (b) $\phi = \pi/2$.

$\phi = \pi/2$ as a function of intensity I_0 for a 100 fs pulse. We have not illustrated the corresponding schemes for DH^+, TH^+, HD^+, and HT^+ because they are mostly the same as H_2^+ in this "shorter" wavelength regime, showing no difference between the two different orientations of each species, contrary to the "long-"wavelength regime illustrated in Figure 4. This is due to the fact that the permanent dipole moment of these heteronuclear species is ineffective when the radiation frequency is high compared to the nuclear motion, as is the case with a simple 1064 nm wavelength excitation. Compared to Figure 4 for the longer wavelengths (CO_2, 10.6 + 5.3 μm), we note that at the shorter wavelengths (YAG, 1064 + 532 nm), Figure 9, the forward/backward ratio is now $P_+/P_- > 1$. This is a complete *reversal* of the long-wavelength (CO_2) results where $P_+/P_- < 1$. We have added in Figure 9b, the P_+/P_- dissociation probabilities for the $\phi = \pi/2$ case where the field is now periodically symmetric (Figure 2b) but is locally asymmetric about each maxima/minima. In this case, the forward/backward ratio is $P_+/P_- < 1$ with a maximum asymmetry $P_+/P_- \simeq 10$ around $I_0 = 4 \times 10^{13}$ W/cm^2, i.e. the complete reverse of the $\phi = 0$ case. When compared to the CO_2 wavelength excitation, Figures 4 and 5, we see again complete reversal of the asymmetry in going from low frequency (CO_2) to higher frequency (YAG) in both $\phi = 0$ and $\pi/2$ cases.

Like Figures 6 and 8, Figure 10 illustrates the logarithm of the electron density integrated over all nuclear positions (i.e. $\ln[\int|\Psi(z,R,t)|^2\, dR]$) at different times during the dissociative ionization. These exact non-Born−Oppenheimer electron distributions show clearly the laser-induced localization of the electron on the backward proton ($z < 0$), while the molecular ion dissociates at $\phi = 0$ (Figure 10a) and on the forward proton ($z > 0$), while it dissociates at $\phi = \pi/2$ (Figure 10b). Again, ionization bursts occur when the dissociating molecular ion reaches the critical distance $R \approx R_c \simeq 8$ au, asymmetrically in the $\phi = 0$ case and symmetrically in the $\phi = \pi/2$ case. This is in agreement with the ratio of the maxima and minima of the net electric field for the $\phi = 0$ and $\phi = \pi/2$ cases, as shown in Figure 2b.

The nonlinear photoelectron spectra, called ATI spectra, for the λ_{YAG} excitation are illustrated in Figures 11 and 12 for $\phi = 0$ and $\phi = \pi/2$, respectively. We have included the results for D_2^+ in order to demonstrate the effect of nuclear time scales. In subfigures a−d of both Figures 11 and 12, the molecule was initialized in the vibrational eigenstate corresponding to $\nu = 5$. In Figure 11, we have added the electron spectra obtained by initializing H_2^+ in $\nu_0 = 1$ (e) and in a superposition of eigenstates (f) corresponding to the Franck−Condon projection from the ground state ($\nu = 0$) of H_2(neutral). Even though the vertical projection from $H_2(\nu{=}0)$ mostly populates the $\nu = 1$, 2, and 3 vibrational levels of H_2^+,[34] we see by comparing Figure 11a,e,f that ionization in the Franck−Condon case (f) is much closer to $\nu_0 = 5$ (a) than to $\nu_0 = 1$. Thus for $\phi = 0$ the experimental measured electron signal would be mainly forward (Figure 11), whereas at $\phi = \pi/2$ this is mainly backward (Figure 12). The ionization asymmetry is even higher for the most energetic electrons. In fact, if one takes only into account electrons with a kinetic energy higher than eight photons, the $P_+/P_{tot.}$ ionization ratio becomes 0.37, 0.22, 0.18, and 0.11 for H_2^+, DH^+, TH^+, and D_2^+, respectively, when $\phi = \pi/2$. This is in agreement with experiments by Rottke et al.[43] Figure 11 shows *no* isotope effect on the ionization asymmetry. In the $\phi = 0$ case, only the total ionization rate is affected and the highest signal is obtained for the molecular ion with the highest reduced mass, D_2^+. This is seen as a consequence of charge resonance enhanced ionization. D_2^+ being the heaviest molecule, it indeed spends more time in the critical region, near $R \simeq R_c$, and thus undergoes more ionization. The $\phi = \pi/2$ case does not show such a regularity. This is probably due to the fact that ionization, in the $\phi = \pi/2$ case, happens equally at both extrema of the field and on a longer time scale than in the $\phi = 0$ case, where the ionization mostly happens at the top of the sharp positive maxima of the field (Figure 2b).

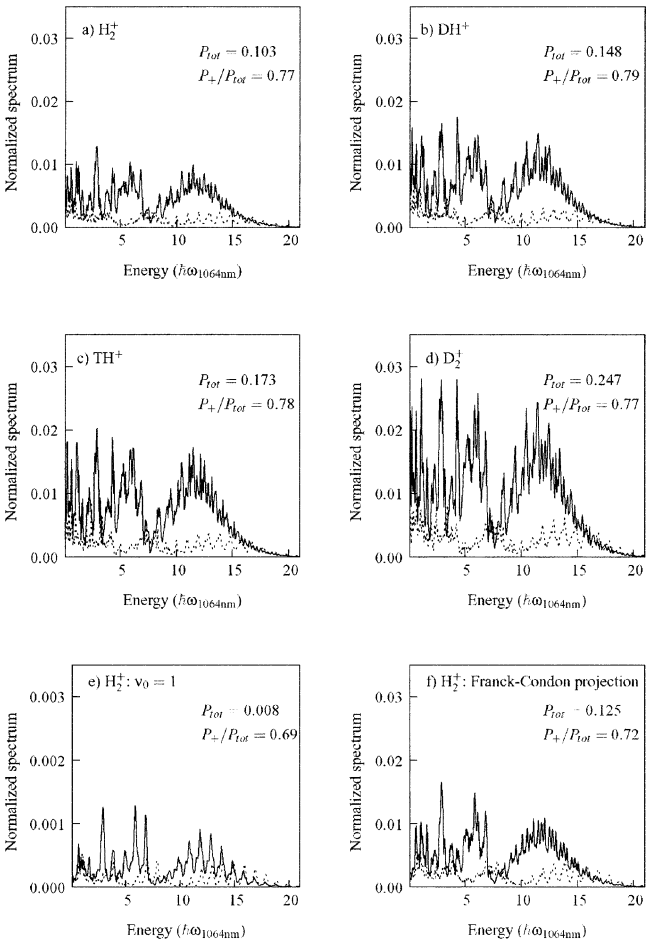

Figure 11. ATI spectra calculated for (a) H_2^+, (b) HD^+, (c) HT^+, and (d) D_2^+ in a 100 fs laser pulse with $\lambda = 1064 + 532$ nm, $\phi = 0$, $f = 0.5$, and $I_0 = 4.4 \times 10^{13}$ W/cm^2. The two last figures show the spectra obtained for the same laser parameters but using different initial vibrational states (ν_0) of H_2^+: (e) $\nu_0 = 1$; (f) Franck−Condon projection from the vibrational ground state ($\nu = 0$) of H_2 (neutral). On these figures, both the *forward* and *backward* ionization channels are shown.

The low-energy proton spectra, illustrated in Figures 13 and 14 for $\phi = 0$ and $\phi = \pi/2$, respectively, are called above threshold dissociation spectra, ATD, as those correspond to nonlinear, multiphotonic dissociation into the repulsive $1\sigma_u$ molecular state.[11] It is remarkable that in the $\phi = 0$ case (Figure 13), the forward subchannel in the ATD spectra becomes less important as the reduced mass of the molecular ion gets higher, while the backward component in the ATD spectra remains essentially the same. This is a clear indication that, in the $\phi = 0$ case, the ionization depopulates the *forward* ATD subchannel preferentially. The combination of this preferential ionization and of the isotopic dependence of the total ionization rates (Figure 11) indicate a clear isotopic effect in the coupling of the ATI and ATD processes when the relative phase of the two harmonics in the laser field are set to $\phi = 0$. When the relative phase is set to $\phi = \pi/2$, the total ionization varies much less regularly with the reduced mass of the molecular ion, as shown

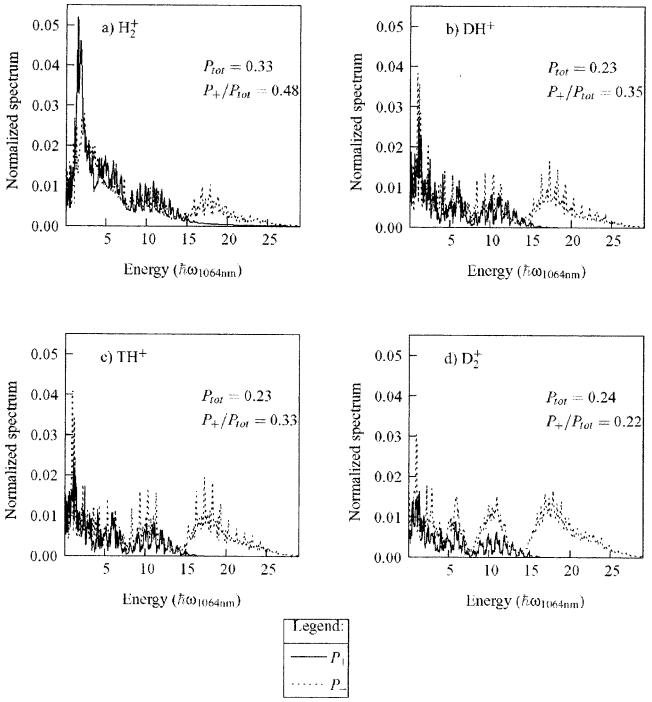

Figure 12. Similar to Figure 11, but with $\phi = \pi/2$ and $I_0 = 5.0 \times 10^{13}$ W/cm^2.

in Figure 12, and consequently the ATD spectra (Figure 14) cannot be interpreted simply.

Finally in Tables 1 and 2, we compare the effect of ionization on the ATD spectra of H_2^+ at various intensities in the 1064 + 532 nm (YAG) regime, as given by the complete, non-Born−Oppenheimer dissociative-ionization calculations. The tables contain the respective populations and asymmetry in the ATI and ATD channels calculated at the end of each pulse. In the last column is displayed the asymmetry in the ATD channel given by the two-surface calculations (i.e. *not* including ionization). We see from these tables that, for H_2^+, the asymmetry in the ATD channel given by the two-surface calculations remains very close to the asymmetries given by the complete dissociative-ionization calculations, up to intensities of $I_0 = 4.4 \times 10^{13}$ W/cm^2 for $\phi = 0$ and $I_0 = 7.7 \times 10^{13}$ W/cm^2 for $\phi = \pi/2$.

Previous coherent-control calculations[39] on possible isotope separation of photodissociating fragments of HD^+ with CO_2 pulses described by eq 3 were limited to two-surface calculations similar to those shown in Figures 4 and 5. In Figures 6 and 8 we have illustrated for λ_{CO_2} and both $\phi = 0$ and $\phi = \pi/2$ that, at $I_0 = 5 \times 10^{13}$ W/cm^2, ionization occurs with a probability $P_i < 10\%$. Thus, under such intensity conditions, one can surmise that a two-surface model would be inadequate because of the effect of ionization. Nevertheless, Tables 1 and 2 show that total ionization of more than 10% occurs for intensities $I_0 > 4 \times 10^{13}$ W/cm^2 for $\lambda = 1064 + 532$ nm excitation. We conclude that ionization will be negligible and two-surface models should be adequate for intensities $I_0 < 4 \times 10^{13}$ W/cm^2 for both λ_{CO_2} and λ_{YAG} in combination with their second harmonics.

4. Discussion and Conclusion

We have presented in the previous sections numerical results for non-Born−Oppenheimer TDSE simulations of dissociative ionization for the isotopomers H_2^+, HD^+, and HT^+ using a two-color coherent control scheme described by the field eq 3. The numerical results illustrate the importance of time scales in the

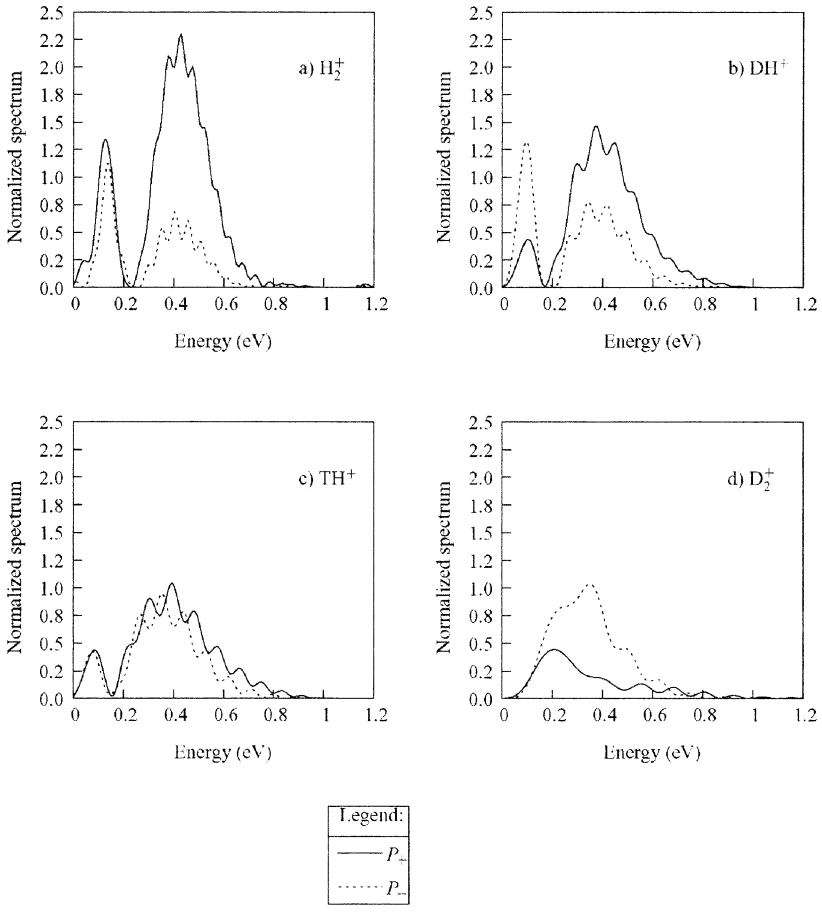

Figure 13. ATD spectra corresponding to the results shown in Figure 11 ($\phi = 0$). Both the *forward* and *backward* dissociation channels are shown.

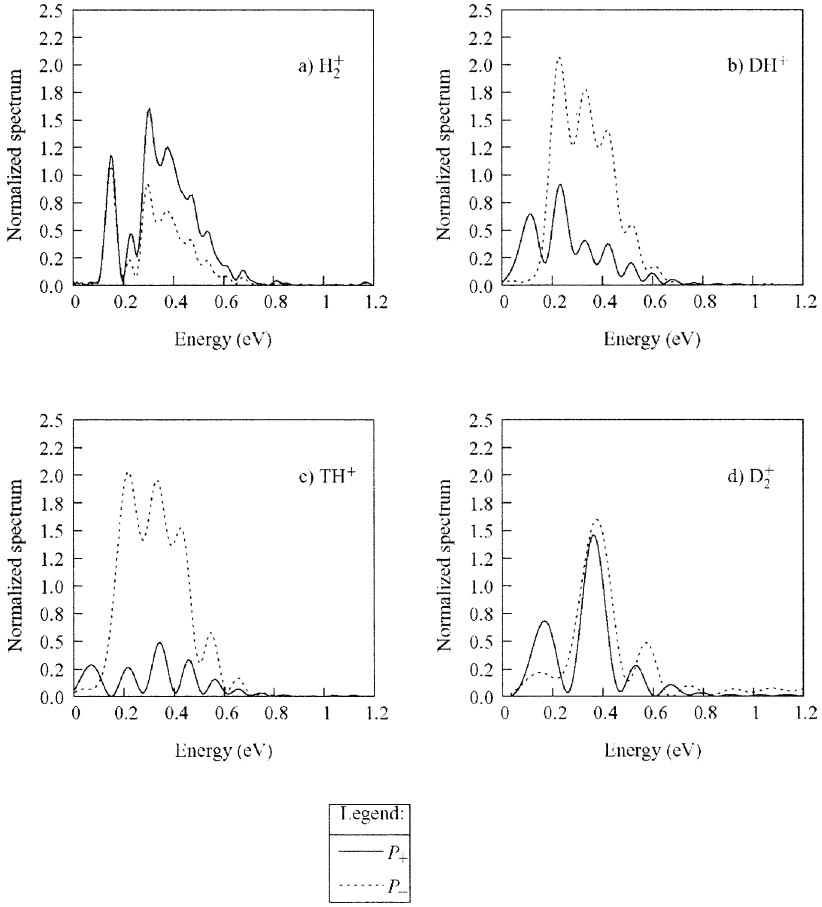

Figure 14. ATD spectra corresponding to the results shown in Figure 12 ($\phi = 1.57$). Both the *forward* and *backward* dissociation channels are shown.

TABLE 1: Populations and Asymmetry in the ATI and ATD Channels for H_2^+ and the Laser Pulse Parameters (See Equation 3), for $\phi = 0$, $\lambda = 1064 + 532$ nm, $f = 0.5$, and Various I_0 Values[a]

	ionization (ATI) ($2p^+ + e^-$ channel)		dissociation (ATD) ($H + p^+$ channel)		
I_0 (W/cm^2)	total	$P_+/(P_+ + P_-)$	total	$P_+/(P_+ + P_-)$ (ion.)	$P_+/(P_+ + P_-)$ (ion.)
4.4×10^{13}	0.11	0.77	0.86	0.75	0.74
6.0×10^{13}	0.46	0.80	0.52	0.40	0.22
1.0×10^{13}	0.85	0.76	0.12	0.77	0.23

[a] For the dissociation channel, the results of the complete calculations (with ionization) are compared to the results of the strictly dissociative calculations (with no ionization).

TABLE 2: Results Similar to Those in Table 1, but for $\phi = \pi/2$ and Different Intensities

	ionization (ATI) ($2p^+ + e^-$ channel)		dissociation (ATD) ($H + p^+$ channel)		
I_0 (W/cm^2)	total	$P_+/(P_+ + P_-)$	total	$P_+/(P_+ + P_-)$ (ion.)	$P_+/(P_+ + P_-)$ (ion.)
4.0×10^{13}	0.08	0.37	0.74	0.09	0.08
5.8×10^{13}	0.35	0.38	0.64	0.24	0.27
7.7×10^{13}	0.71	0.35	0.28	0.54	0.55
8.0×10^{13}	0.64	0.25	0.34	0.62	0.54

dissociative-ionization process. Thus, with CO_2 laser excitation in combination with its second harmonic, the two important time scales are the laser period $t_{CO2} = 35$ fs as compared to the proton time scale $t_p = 15$ fs. In this case the proton motion is faster than the laser period, thus allowing the proton to sample more efficiently the field structure illustrated in Figure 2b. As a result for the low CO_2 frequency, electrons follow the fields *adiabatically*; i.e. electron transfer occurs in the opposite direction of the field sign, thus shielding the protons and creating dissociation asymmetries. Thus, in the case of H_2^+, DH^+, and TH^+ aligned with the field, the main dissociation products (Figure 4a−c) are predicted to be H^+, D^+, and T^+ in the backward direction for the $\phi = 0$ field configuration. This is due to the longer negative field amplitude at $\phi = 0$ which transfers the electron to the right nucleus ($z > 0$). As the intensity increases, this effect diminishes and the more intense but shorter positive field amplitude begins to act and diminishes the asymmetry. In the $\phi = \pi/2$ field configuration, where the field is globally symmetric, one would expect no asymmetry to occur in the photodissociation. The largest asymmetry nevertheless occurs, leading to D^+ and T^+ forward products (Figure 5d,e), contrary to the $\phi = 0$ results discussed above. As shown in Figure 6, this is due to localization of the electron on the left nucleus ($z < 0$) even in the presence of ionization, resulting in a large forward proton asymmetry in H_2^+ (see Figure 4a). The slower dissociation of HD^+ and HT^+ into $H + D^+$ and $H + T^+$ (as opposed to DH^+ and TH^+ into $D + H^+$ and $T + H^+$) where the latter have larger dipole moments (see Figure 3) enhances the electron transfer to the left nucleus, especially at larger internuclear distances where the electron-transfer rate decreases. Thus, Figures 4 and 5 show that the dipole moments of the isotopomers HD^+ and HT^+ act in opposite direction in the phase configuration $\phi = 0$ and $\phi = \pi/2$. At $\phi = 0$, less dissociation into $H + D^+$ and $H + T^+$ occurs, leading to preferential emission of D^+ and T^+ in the backward direction because of the smaller dipole moments, whereas, at $\phi = \pi/2$, this slower dissociation enhances the electron transfer and results in more

D^+ and T^+ production in the forward direction. The dissociation results shown in Figure 8, and the electron density evolution shown in Figure 8 for $\phi = \pi/2$ suggest it is the positive field amplitude which dominates the electron and nuclear dynamics; i.e. even though the change from the negative ($E < 0$) to positive ($E > 0$) field amplitude is rapid, because of the slow field period ($t_{CO2} > t_p$), the electrons and nuclei adjust rapidly (or *adiabatically*) to this field change. This adiabatic response of electrons and nuclei to the slower time-dependent field configurations illustrated in Figure 2b allows for a quasistatic interpretation of the dissociation of the isotopomers in the low-frequency CO_2 case.

As the field frequency is increased leading to shorter laser periods, the results in Figures 9−14 show a complete reversal of the dissociative ionization asymmetries. Thus, for $\lambda = 1064$ nm, $t_{YAG} = 3.5$ fs, and one is in the fast field regime, $t_{YAG} < t_p$, and one no longer expects the electrons *and* protons to follow the field. This reversal of asymmetries is clearly seen in the electron probability evolution illustrated in Figure 10, where at $\phi = 0$ the electron is localized mainly on the left nucleus ($z < 0$) and at $\phi = \pi/2$ it is mainly on the right nucleus ($z > 0$). Thus, now, contrary to the CO_2 case (Figures 6 and 8), at $\phi = 0$ the electron responds to the positive field amplitude and conversely, at $\phi = \pi/2$, the electron behavior is dominated by the negative field and is consequently transferred to the right nucleus. This contrary response as compared to the low-frequency and longer period CO_2 laser regime can be explained in terms of the *nonadiabatic* electron transfer induced by the faster YAG laser field. As shown previously, any two-level system in a time-dependent field, i.e. with the time t as the evolution parameter, can be described as a nonadiabatic system where time-dependent transitions become equivalent to nonadiabatic transitions between molecular potentials with the internuclear distance R as the evolution parameter.[44−47] Thus, in the time-dependent case, we can define a nonadiabatic mixing angle θ, where

$$\Psi(t) = \cos\theta(t)|1\rangle + \sin\theta(t)|2\rangle \qquad (15)$$

is the coherent state created by a time-dependent field $E(t)$ coupling the two states $|1\rangle$ and $|2\rangle$ through the radiative coupling $\mu E(t)$. The corresponding nonadiabatic coupling becomes[46,47]

$$\frac{\partial\theta}{\partial t} = \frac{\mu}{\Delta\epsilon}\left(\frac{\partial E(t)}{\partial t}\right)(\cos(2\theta))^2 \qquad (16)$$

where μ is the transition moment and $\Delta\epsilon = \epsilon_2 - \epsilon_1$. Examination of Figure 2b shows that, for $\phi = \pi/2$, since the field is globally symmetric, no localization of the electron should occur upon dissociation. However the electron responds nonadiabatically, i.e. remains localized on the right nucleus due to the negative field amplitude, because it cannot respond adiabatically to the positive field amplitude due to the rapid rise (and therefore larger variation $\partial E/\partial t$ in the field). For the $\phi = 0$ configuration, contrary to the CO_2 excitation case, because of the different time scales $t_{YAG} < t_p$, the proton motion is slow compared to the field variations. Response to the much weaker negative field amplitude is dominated by the stronger positive field amplitude, thus enhancing electron localization on the left nucleus and resulting in forward proton dissociations.

In conclusion we have shown that two different dynamical regimes occur in dissociative ionization of the molecule H_2^+ and its isotopomers as a function of the wavelength of two-color short laser pulse excitation. The first, *adiabatic* regime is obtained when the laser period is longer than the nuclear period as for CO_2 excitation. In this case, electrons and nuclei respond to a slowly varying quasistatic field and the dissociation can be explained using quasistatic models of electron transfer and dissociation by *barrier suppression*. In this regime, dipole moments influence strongly the dissociative process, especially at intensities $I_0 < 2 \times 10^{13}$ W/cm^2 and pulse lengths shorter than 100 fs, where ionization is negligible. In this intensity regime, H^+ production dominates for the DH^+ and TH^+ molecular orientations at $\phi = 0$ (Figure 4), whereas D^+ and T^+ are dominant products at $\phi = \pi/2$ (Figure 6) for HD^+ and HT^+ orientations. Higher intensities than 2×10^{13} W/cm^2 and longer pulses lead to loss of isotope selectivity due to competition between ionization and dissociation.

At $\lambda = 1063 + 532$ nm excitation, the laser period $t_{YAG} = 3.5$ fs is now faster than proton motion ($t_p = 15$ fs). On dissociation, because of the decrease of the electron-transfer rate at larger distances, one enters a *nonadiabatic* regime. Thus, electron localization on one nucleus is enhanced by large variations of the field amplitude. Although dipole moments have little influence on the dissociative-ionization dynamics, the nuclear time scales now control the asymmetry of the dissociation. H_2^+ with the fastest nuclear time scale allows for the dissociating nuclei to reach more quickly the larger distances at which the electron-transfer rates are slower. This increases electron nonadiabatic effects resulting in stronger localization of the electrons. It is at these larger distances, approaching the critical distance R_c for charge resonance enhanced ionization, that we have shown previously that ionization can be best controlled by phase variations of the $\omega + 2\omega$ field combination described by eq 3.[47]

Acknowledgment. We thank the Canadian Institute for Photonic Innovations (CIPI) for financing this research.

References and Notes

(1) Brabec, T.; Krausz, F. *Rev. Mod. Phys.* **2000**, *72*, 545.
(2) Hentschel, M.; Kienberger, R.; Spielmann, C.; Reider, G. A.; Milosevic, N.; Brabec, T.; Corkum, P.; Heinzmann, U.; Drescher, M.; Krausz, F. *Nature* **2001**, *414*, 509.
(3) Bandrauk, A., Fujimura, Y., Gordon, R., Eds.; *Laser Control and Manipulation of Molecules*; ACS Symposium Series 821; American Chemical Society: Washington, D. C., 2002.
(4) Rice, S.; Zhao, M. *Optical Control of Molecular Systems*; John Wiley & Sons Inc.: New York, 2000.
(5) Brumer, P.; Shapiro, M. *Molecules in Laser Fields*; Marcel Dekker Publications: New York, 1994; Chapter 6.
(6) Brumer, P.; Shapiro, M. *Chem. Phys. Lett.* **1986**, *126*, 541.
(7) Brumer, P.; Hepburn, J.; Shapiro, M. *Chem. Phys. Lett.* **1988**, *149*, 451.
(8) Aubanel, E.; Bandrauk, A. *Chem. Phys. Lett.* **1995**, *229*, 169.
(9) Bandrauk, A.; Aubanel, A. *Chem. Phys. Lett.* **1995**, *198*, 159.
(10) Haljan, P.; Ivanov, M. Y.; Corkum, P. B. *Laser Phys.* **1997**, *7*, 839.
(11) Bandrauk, A. *Molecules in Laser Fields*; Marcel Dekker Publications: New York, 1994; Chapter 1, p 3.
(12) Keldysh, K. *JETP* **1965**, *20*, 1307.
(13) Gavrila, M., Ed. *Atoms in Intense Laser Fields*; Academic Press: New York, 1992.
(14) Corkum, P. *Phys. Rev. Lett.* **1993**, *71*, 1994.
(15) De Witt, M.; Lewis, R. *J. Chem. Phys.* **1998**, *108*, 1.
(16) Scrinzi, A.; Brabec, T. *Phys. Rev. Lett.* **1999**, *83*, 706.
(17) Zuo, T.; Chelkowski, S.; Bandrauk, A. *Phys. Rev. A* **1993**, *48*, 3837.
(18) Zuo, T.; Bandrauk, A. *Phys. Rev. A* **1995**, *52*, 2511.
(19) Chelkowski, S.; Atabek, O.; Bandrauk, A. *Phys. Rev. A* **1996**, *54*, 3235.
(20) Chelkowski, S.; Bandrauk, A. *J. Phys. B* **1995**, *28*, L723.
(21) Chelkowski, S.; Foisy, C.; Bandrauk, A. *Int. J. Quantum Chem.* **1997**, *65*, 503.
(22) Seideman, T.; Ivanov, M.; Corkum, P. *Phys. Rev. Lett.* **1995**, *75*, 2819.
(23) Mulliken, R. *J. Chem. Phys.* **1939**, *7*, 20.
(24) Yu, H.; Bandrauk, A. D. *J. Phys. B* **1998**, *31*, 1533.
(25) Bandrauk, A.; Ruel, J. *Phys. Rev. A* **1999**,

(26) Kawata, I.; Kono, H.; Bandrauk, A. *Phys. Rev. A* **2000**, *62*, 031401.
(27) Constant, E.; Stapelfeldt, H.; Corkum, P. *Phys. Rev. Lett.* **1996**, *76*, 4140.
(28) Gibson, G.; Li, M.; Guo, C.; Neira, J. *Phys. Rev. Lett.* **1999**, *79*, 2022.
(29) Schmidt, M.; Cornaggia, C.; Normand, D. *Phys. Rev. A* **1994**, *50*, 5037.
(30) Schumacher, D.; Bucksbaum, P. *Phys. Rev. A* **1996**, *54*, 4271.
(31) Sheehy, B.; Walker, B.; DiMauro, L. *Phys. Rev. Lett.* **1995**, *74*, 4799.
(32) Thompson, M.; Thomas, M.; Taday, P.; Posthumus, J.; Langley, A.; L. J., F.; Codling, K. *J. Phys. B* **1997**, *30*, 5755.
(33) Bandrauk, A.; Chelkowski, S. *Phys. Rev. Lett.* **2000**, *84*, 3562.
(34) Chelkowski, S.; Zamojski, M.; Bandrauk, A. *Phys. Rev. A* **2001**, *63*, 023409.
(35) Dietrich, P.; Corkum, P. *J. Chem. Phys.* **1992**, *97*, 3187.
(36) Conjusteau, A.; Bandrauk, A.; Corkum, P. *J. Chem. Phys.* **1997**, *106*, 9095.
(37) Hiskes, J. *Phys. Rev.* **1961**, *122*, 1207.
(38) Hanson, G. *J. Chem. Phys.* **1975**, *62*, 1161.
(39) Charron, E.; Giusti-Suzor, A.; Mies, F. *Phys. Rev. Lett.* **1995**, *75*, 7815; *J. Chem. Phys.* **1995**, *103*, 7359.
(40) Dion, C.; Keller, A.; Atabek, O.; Bandrauk, A. *Phys. Rev. A* **1999**, *59*, 1382.
(41) Cai, L.; Marango, J.; Friedrich, B. *Phys. Rev. Lett.* **2001**, *86*, 775.
(42) Hoki, K.; Fujimura, Y. *Chem. Phys. Lett.* **2001**, *267*, 187.
(43) Rottke, H.; Ludwig, J.; Sandner, W. *Phys. Rev. A* **1996**, *54*, 2224.
(44) McCann, J.; Bandrauk, A. *Phys. Lett. A* **1991**, *151*, 509.
(45) Kayanuma, Y. *Phys. Rev. B* **1993**, *47*, 9940.
(46) Bandrauk, A.; Kono, H. In *Advances in Multiphoton Spectroscopy*; Lin, S. H., Ed.; Elsevier Publications: submitted for publication.
(47) Bandrauk, A.; Yu, H. *Int. J. Mass Spectrom.* **1999**, *192*, 379.